

Phonon Mediated Off-Resonant Quantum Dot-Cavity Coupling

Arka Majumdar,^{*} Yiyang Gong, Erik D. Kim, and Jelena Vučković

¹*E.L. Ginzton Laboratory,
Stanford University, Stanford, CA, 94305*

A theoretical model for the phonon-mediated off-resonant coupling between a quantum dot and a cavity, under resonant excitation of the quantum dot, is presented. We show that the coupling is caused by electron-phonon interaction in the quantum dot and is enhanced by the cavity. We analyze recently observed resonant quantum dot spectroscopic data by our theoretical model.

One of the interesting recent developments in cavity quantum electrodynamics (CQED) experiments with quantum dots (QDs) coupled to semiconductor microcavities is the observation of off-resonant dot-cavity coupling. This unusual phenomenon is observed both in photoluminescence studies, where an above-band laser generates carriers that incoherently relax to recombine at the QD frequency [1–3] and also under resonant excitation of the QD or the cavity [4, 5]. The coupling observed via photoluminescence is attributed to several phenomena including pure QD dephasing [6], the electron-phonon interaction [7, 8], multi-exciton complexes [9] and charges in the vicinity of the QD [10]. To isolate the role of phonons in off-resonant QD-cavity coupling, studies employing resonant excitation of the QD are preferable as they avoid possible complications arising from multi-excitonic complexes and nearby charges generated in above band pumping. Resonant excitation of a QD coupled to an off-resonant cavity has been recently used to perform QD spectroscopy, enabling the observation of power broadening of the QD line-width and saturation of the cavity emission [11–13]. However, there is presently no theoretical model accounting for off-resonant dot-cavity coupling for the case of resonant QD excitation. Although off-resonant coupling can be modeled by introducing a phenomenological incoherent cavity pumping mechanism [14], such a treatment masks the actual physical phenomenon responsible for the coupling. Without an explicit coherent driving term in the system Hamiltonian, the resonant QD spectroscopy results cannot be explained.

In this Letter, we theoretically model the phonon-mediated interaction between a cavity mode and an off-resonant QD under resonant excitation of the QD. We first model the coupling via pure QD dephasing. Then, we propose a new model where the phonon-mediated coupling is enhanced by the presence of the cavity. We compare these two models and find that they provide qualitatively similar signatures in terms of experimental resonant QD spectroscopic studies, such as power broadening and saturation of a resonantly driven QD [11, 12]. However, in the newly proposed model, the coupling is main-

tained at very large QD-cavity detunings (~ 3 meV), as observed in the recent experiments [11]. We also observe the signature of the inherent asymmetry between phonon emission and absorption rate in the simulated QD spectroscopy results, depending on whether the QD is red or blue detuned from the cavity.

The dynamics of a coherently driven QD (with a ground state $|g\rangle$ and an excited state $|e\rangle$) coupled to an off-resonant cavity mode is governed by the Hamiltonian H (in a frame rotating at the driving laser frequency)

$$H = \Delta\omega_c a^\dagger a + \Delta\omega_a \sigma^\dagger \sigma + ig(a^\dagger \sigma - a \sigma^\dagger) + \Omega(\sigma + \sigma^\dagger) \quad (1)$$

where, a and σ are the annihilation and lowering operators for the cavity mode and the QD, respectively; $\Delta\omega_c = \omega_c - \omega_l$ and $\Delta\omega_a = \omega_a - \omega_l$ are the cavity and dot detunings from the driving laser, respectively; $\Delta = \omega_a - \omega_c$ is the QD-cavity detuning; Ω is the Rabi frequency of the driving laser and is proportional to the laser field amplitude and g is the coherent interaction strength between the QD and the cavity.

In this coupled system, there are two independent mechanisms for energy dissipation: cavity decay and QD dipole decay. The system losses can be modeled by the Liouvillian, and the Master equation describing the dynamics of the lossy system is given by

$$\frac{d\rho}{dt} = -i[H, \rho] + 2\kappa\mathcal{L}[a] + 2\gamma\mathcal{L}[\sigma] \quad (2)$$

where ρ is the density matrix of the coupled QD-cavity system, 2γ and 2κ are the QD spontaneous emission rate and the cavity population decay rate, respectively. We neglect any non-radiative decay of the QD exciton. $\mathcal{L}[D]$ is the Lindblad operator corresponding to a collapse operator D and is given by:

$$\mathcal{L}[D] = D\rho D^\dagger - \frac{1}{2}D^\dagger D\rho - \frac{1}{2}\rho D^\dagger D \quad (3)$$

In addition, phonons in the solid state system destroy the coherence of the exciton. This is generally modeled by adding an additional incoherent decay term $2\gamma_d\mathcal{L}[\sigma^\dagger\sigma]$ to the Master equation, where $2\gamma_d$ is the pure dephasing rate of the QD. This term destroys the polarization of the QD without affecting the population of the QD. The dissipation of the QD polarization and population ($\sigma_z =$

^{*}Electronic address: arkam@stanford.edu

$[\sigma^\dagger, \sigma]$ is given by the following mean-field equations:

$$\frac{d\langle\sigma\rangle}{dt} = -(\gamma + \gamma_d)\langle\sigma\rangle \quad (4)$$

$$\frac{d\langle\sigma_z\rangle}{dt} = -2\gamma(1 + \langle\sigma_z\rangle) \quad (5)$$

Hence, the linewidth of the QD, at the zero excitation power limit, is given by $2(\gamma + \gamma_d)$. However, in this model, the effect of phonons is embedded in the phenomenological pure dephasing rate γ_d , which affects only the QD, and does not include any cavity effects.

We now propose a different model for off-resonant dot-cavity coupling, where the phonon-mediated coupling strength is affected by both the cavity and the QD. The effect of phonons can be modeled by replacing the pure dephasing term with two additional incoherent decay terms in the Master equation. For blue-detuned QD (Fig. 1 a) we have:

$$\begin{aligned} \frac{d\rho}{dt} = & -i[H, \rho] + 2\kappa\mathcal{L}[a] + 2\gamma\mathcal{L}[\sigma] \\ & + 2\gamma_r\bar{n}\mathcal{L}(\sigma^\dagger a) + 2\gamma_r(\bar{n} + 1)\mathcal{L}(\sigma a^\dagger) \end{aligned} \quad (6)$$

where, $2\gamma_r$ is an effective decay rate of the QD excitation states via the emission of a phonon and a photon at the off-resonant cavity frequency. \bar{n} is the average number of phonons at the dot-cavity detuning frequency (Δ) present in the system at thermal equilibrium with the reservoir at a temperature T , and is given by

$$\bar{n}(\Delta, T) = \frac{1}{e^{\hbar\Delta/k_B T} - 1} \quad (7)$$

The analysis for a QD red detuned from the cavity (Fig. 1 b) can be carried out in a similar manner by replacing the final two terms of Eqn.6 with $2\gamma_r\bar{n}\mathcal{L}(\sigma a^\dagger)$ and $2\gamma_r(\bar{n} + 1)\mathcal{L}(\sigma^\dagger a)$.

The decay term $\sigma^\dagger a$ denotes the annihilation of a cavity photon and excitation of the QD, while the term σa^\dagger denotes the creation of a cavity photon and collapse of the QD to its ground state, accompanied by the creation (or annihilation) of phonons to compensate for the QD-cavity frequency difference. Only the second process is important for observing cavity emission under resonant excitation of the dot. We also note that the observation of QD emission under resonant excitation of the cavity [4] can be modeled in the same way by changing the coherent driving term from $\Omega(\sigma + \sigma^\dagger)$ to $\Omega(a + a^\dagger)$. In this situation, the collapse operator $\sigma^\dagger a$ is important. Similar decay channels have been proposed to model cavity assisted atomic decay [15]. A detailed derivation of these incoherent terms can be found in the Supplementary Materials. We call this process a cavity-enhanced phonon process.

We first consider the case where the QD is blue detuned from the cavity (Fig. 1 a). The qualitative nature of the dissipation of the QD polarization and population can be determined by the mean-field equations (assuming $\bar{n} = 0$,

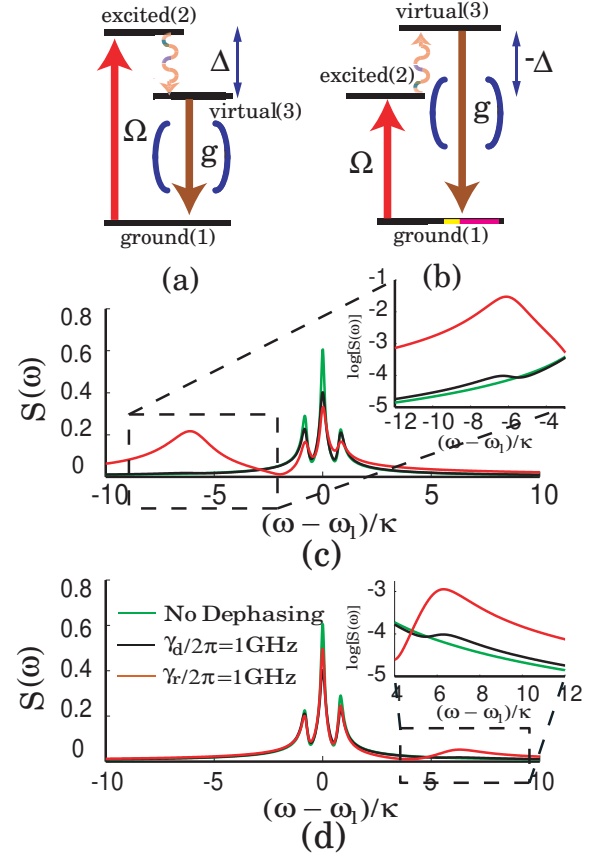


FIG. 1: (a),(b) Level diagram of the coupled QD/cavity system for blue (a) and red (b) detuned QD relative to the cavity resonance. A laser drives the quantum dot (transition between ground state (1) and excited state (2)) resonantly. The excited state (2) can decay via two paths: the first is by direct decay back to the ground state (1) via the spontaneous emission of the QD; the second is by indirect decay via the emission (Fig. 1a) or absorption (Fig. 1b) of a phonon (transition (2) to (3)) and subsequent emission of a photon at the cavity frequency (transition (3) to (1)). (c), (d) Emission $S(\omega)$ as a function of frequency ω for a QD resonantly driven by a laser ($\Delta\omega_a = 0$). The plot (c) corresponds to a QD that is blue detuned, and (d) corresponds to a QD that is red detuned from the cavity. Three different cases are considered: first, without any dephasing; second with pure dephasing and third with a cavity enhanced phonon process (our newly introduced model). We observe the Mollow triplet at the QD frequency in all three cases. The inset of (c) and (d) show an enlarged view of the emission at the cavity frequency. We observe no off-resonant cavity emission without pure dephasing, or our newly introduced cavity enhanced phonon process. For the simulation we assume $g/2\pi = \kappa/2\pi = 20$ GHz; $\gamma/2\pi = 1$ GHz; $\Omega/2\pi = 6$ GHz; QD-cavity detuning $\Delta/2\pi = \pm 6$ GHz.

i.e., at the zero temperature limit):

$$\frac{d\langle\sigma\rangle}{dt} = -\gamma\langle\sigma\rangle - \gamma_r(1 + \langle a^\dagger a \rangle)\langle\sigma\rangle \quad (8)$$

$$\frac{d\langle\sigma_z\rangle}{dt} = -2\gamma(1 + \langle\sigma_z\rangle) - 2\gamma_r(1 + \langle a^\dagger a \rangle)(1 + \langle\sigma_z\rangle) \quad (9)$$

We notice that, unlike the pure dephasing case, both the QD population and polarization are affected by the cavity enhanced phonon process. The linewidth of the QD at the zero excitation power limit is given by $2\gamma + 2\gamma_r(1 + \langle a^\dagger a \rangle)$, which is qualitatively different from what we expect from a pure QD dephasing model (as the presence of cavity photons affects the QD linewidth). We emphasize that for both models, the QD linewidths obtained from the mean-field equations neglect the modification resulting from cavity QED effects in the presence of the cavity and hence the predicted linewidths are only recovered at large QD-cavity detunings.

The resonance fluorescence of the system is given by the power spectral density (PSD) of the coupled system. As we collect the fluorescence primarily from the cavity, the PSD is calculated as the Fourier transform of the cavity field auto-correlation:

$$S(\omega) = \int_{-\infty}^{\infty} \langle a^\dagger(\tau)a(0) \rangle e^{-i\omega\tau} d\tau \quad (10)$$

To determine the two time correlation functions and, subsequently, the PSD, we use the quantum regression theorem [16].

We simulate the coupled system using numerical integration routines provided in the quantum optics toolbox [17] with realistic system parameters $\kappa/2\pi = g/2\pi = 20$ GHz and $\gamma/2\pi = 1$ GHz. The off-resonant coupling is observed both for a strongly ($g > \kappa$) and a weakly coupled QD to the cavity ($g < \kappa$). Figure 1 c shows the numerically calculated resonance fluorescence spectra obtained from the cavity under resonant excitation of a blue detuned QD for three different cases: no dephasing, pure QD dephasing and phonon-induced exciton decay at a bath temperature of 4 K. We first note that no emission is observed at the cavity frequency in the absence of pure dephasing or cavity enhanced phonon process (see inset of Fig. 1 c). Though the pure dephasing ($\gamma_d/2\pi = 1$ GHz) and phonon-induced decay ($\gamma_r/2\pi = 1$ GHz) cases both show off-resonant cavity emission, the latter shows enhanced cavity emission. In all three cases, we also observe the Mollow triplet at the QD frequency, as expected from QD resonance fluorescence [18]. The Mollow side-band closer to the cavity is enhanced compared to the other side-band causing an asymmetric triplet. Fig. 1 d shows the similar spectra for a red-detuned QD. Our model predicts that the emission at cavity frequency is considerably smaller for a red detuned QD compared to a blue-detuned one as expected at finite temperature (as the process for a red-detuned dot relies on phonon absorption, while for a blue-detuned dot relies on phonon emission).

We then perform simulations to observe how the emission collected at the cavity frequency depends on the dephasing and phonon-induced decay rates, as well as on the field of the driving laser resonant with the QD ($\Delta\omega_a = 0$). We observe that the cavity emission I increases almost linearly with the pure QD dephasing rate γ_d [Fig. 2 a], but exhibits a nonlinear dependence on the

rate γ_r when the coupling is enhanced by the presence of the cavity. Fig. 2 b shows the cavity fluorescence as a function of the laser Rabi frequency Ω . For both models, the cavity fluorescence I follows a saturation curve

$$I = I_{sat} \frac{\tilde{P}}{1 + \tilde{P}} \quad (11)$$

where, $\tilde{P} \propto \Omega^2$ and I_{sat} is the saturated cavity emission intensity. As noted previously in the article, the cavity emission is higher when the process is enhanced by the presence of the cavity. Furthermore, we investigate the dependence of the saturation emission intensity I_{sat} as a function of the QD-cavity detuning Δ (Fig. 2 c). I_{sat} falls off as $1/\Delta^2$ with the detuning Δ when the dot-cavity coupling is modeled as a pure dephasing process. However, when the coupling is modeled as a cavity enhanced phonon process, the saturation intensity exhibits a diminished dependence on detuning Δ (estimated to be $\sim 1/\Delta^{0.25}$). Hence, one may observe off-resonant coupling for larger detunings when the phonon process is enhanced by the cavity. Fig. 2 d shows $\log(I)$ as a function of the cavity decay rate κ , for a fixed detuning of $\Delta/2\pi = 200$ GHz. For both models, the emission falls off as $1/\kappa^2$, signifying that the off-resonant coupling does not depend on the overlap between the QD and the cavity spectra.

We now measure the QD line-width $\Delta\omega$ monitoring the cavity emission, while scanning the laser wavelength across the QD resonance, similar to the experiments in Ref. [11]. We observe that at very low excitation power $\Omega/2\pi = 1$ GHz and large QD-cavity detuning $\Delta/2\pi = 12\kappa$, the linewidths of the QD are very close to the theoretical linewidth in the absence of the cavity (shown by the solid black line in Fig. 3 a). At a constant QD-cavity detuning and laser excitation power, the QD line-width increases with increasing γ_d and γ_r (Fig. 3 a). We observe broadening of the line-width with increasing laser power (Figs. 3 b). The power broadened QD linewidth $\Delta\omega$ is fit with the model $\Delta\omega = \Delta\omega_0 \sqrt{1 + \tilde{P}}$, where $\Delta\omega_0$ is the intrinsic line-width of the QD and \tilde{P} is obtained from the fit to the saturation of the cavity emission [11]. The theoretical model does not reproduce the additional power-independent broadening of the QD [11] and we believe that this extra broadening may result from QD spectral diffusion [19]. We analyze the intrinsic QD linewidth $\Delta\omega_0$ (without power broadening, i.e., obtained from plots in Figs. 3 b at $\Omega = 0$ limit) as a function of the dot-cavity detuning Δ for two different models (Figure 3 c). We observe that at large detuning, $\Delta\omega_0$ approaches the unperturbed QD linewidth $2(\gamma + \gamma_d)$ and $2(\gamma + \gamma_r)$, respectively. We fit empirical models of $\Delta^{-\alpha}$ to the intrinsic linewidths for the two models and find that with pure QD dephasing, $\Delta\omega_0$ falls off more slowly ($\alpha \simeq 0.4$) compared to the cavity enhanced coupling ($\alpha \simeq 0.7$). The weak dependence of the intrinsic QD linewidths on the dot-cavity detuning shows that the off-resonant cavity does not perturb the QD significantly.

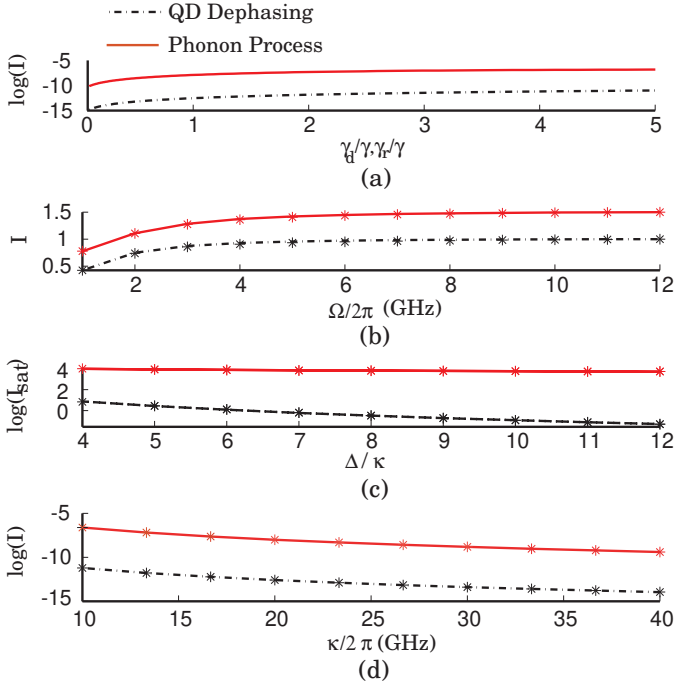


FIG. 2: Resonance fluorescence I collected from the cavity for a blue-detuned QD ($\Delta > 0$). (a) $\log(I)$ as a function of the rates γ_d and γ_r (for two models, respectively). $\Delta/\kappa = 10$. (b) Normalized cavity fluorescence as a function of the Rabi frequency Ω of the laser for two models. Saturation of the cavity emission is observed. The fluorescence values are not in scale. (c) Dependence of the saturated cavity emission I_{sat} on the dot-cavity detuning Δ . (d) $\log(I)$ as a function of the cavity linewidth κ . (Parameters used for all the simulations are $g/2\pi = \kappa/2\pi = 20$ GHz; $\gamma/2\pi = 1$ GHz. For Figs. 2 a, c and d, $\Omega/2\pi = 4$ GHz and for Figs. 2 b, c and d, $\gamma_d/2\pi = \gamma_r/2\pi = 1$ GHz.)

However, the results are dramatically different for a red-detuned QD. This is a result of the fact that the rate of the incoherent process involving the operator σa^\dagger is different depending on whether the QD is red or blue detuned from the cavity (because at any temperature, the rates of absorption and emission of phonons are different). This asymmetry is manifested in both the emission collected at the cavity resonance and in the QD spectroscopy result. Fig. 4 a shows the difference in the QD linewidths as a function of the bath temperature T for different driving laser Rabi frequencies Ω , when the QD is red or blue detuned from the cavity by same absolute value. We observe that the difference in linewidth is higher when the QD is weakly driven and hence is not power broadened. Full quantum optical simulations show that the linewidth depends on the bath temperature, but reaches the maximum value of $2\gamma_r$ at a higher temperature. Fig. 4 b shows the ratio of the cavity emission as a function of the bath temperature for different driving laser Rabi frequencies Ω . The difference in cavity intensity is maximum at lower bath temperature and is almost

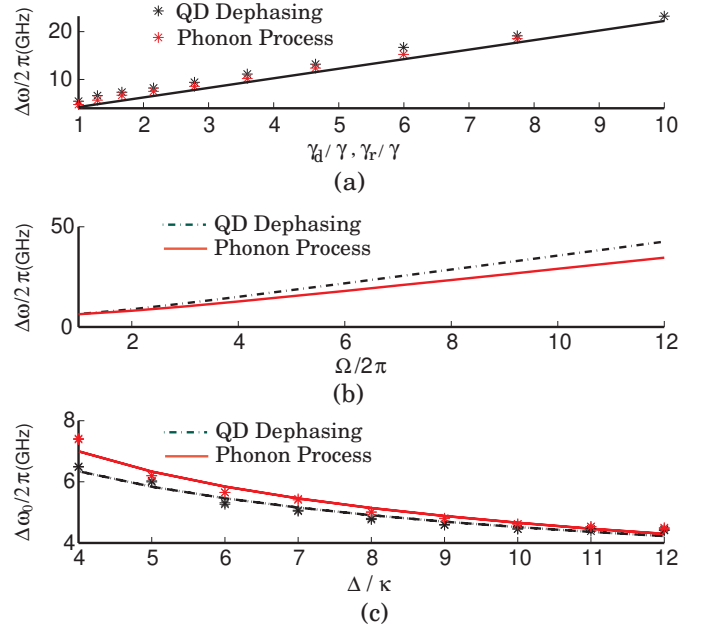


FIG. 3: Linewidth of the blue detuned QD relative to the cavity ($\Delta > 0$) as measured by monitoring the off-resonant cavity emission (similar to the experiments in Ref. [11]). Results obtained from two models are presented. (a) QD linewidth as a function of the rates γ_d and γ_r for pure dephasing and the cavity enhanced phonon process, respectively. In both cases, $\Omega/2\pi = 1$ GHz and $\Delta = 12\kappa$. The solid black line shows the theoretical estimates of the QD linewidth when the laser excitation power is very low and the QD is not significantly perturbed by the cavity. (b) Power broadened linewidth vs laser Rabi frequency Ω for QD-cavity detuning $\Delta/2\pi = 6$ GHz (for the case of pure QD dephasing and the cavity enhanced phonon process). (c) Dependence of the intrinsic QD linewidth $\Delta\omega_0$ on dot-cavity detuning Δ . $\Delta\omega_0/2\pi$ approaches $2(\gamma + \gamma_d)/2\pi$ or $2(\gamma + \gamma_r)/2\pi$ (both chosen to be 4 GHz) with large Δ . (Parameters used for all the simulations are: $\kappa/2\pi = g/2\pi = 20$ GHz; $\gamma/2\pi = 1$ GHz.)

zero at higher temperature.

In conclusion, we have proposed a theoretical model for the off-resonant dot-cavity coupling under resonant excitation of the QD. Introduction of an incoherent decay channel (referred to as the cavity enhanced phonon process, which is different from pure dephasing) shows that the phonon-mediated dot-cavity coupling is enhanced by the presence of the cavity. By comparing the power-broadening and saturation of the QD between the cavity enhanced phonon process and pure QD dephasing, we found that the dot-cavity coupling is enhanced in the former case and is observed for a larger QD-cavity detuning. Our model can also be used to explain asymmetry in the spectroscopy results for a QD blue and red detuned from the cavity. We believe that such an off-resonant dot-cavity coupling can be used as an efficient read-out channel for resonant QD spectroscopy and for QD-spin manipulation.

The authors acknowledge financial support provided

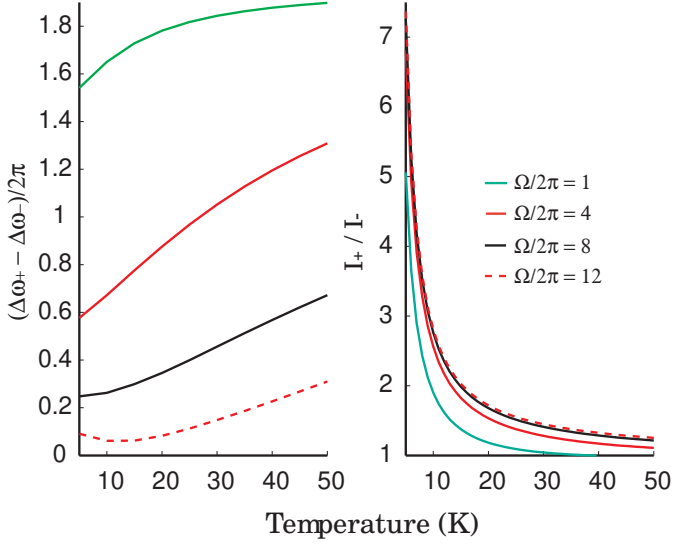


FIG. 4: (a) The difference in QD linewidths measured via collected emission through off-resonant cavity, for a blue ($\Delta\omega_+$) and a red ($\Delta\omega_-$) detuned QD for different values of the excitation laser Rabi frequency Ω as a function of the bath temperature T . (b) Ratio of the cavity intensity for an off-resonant QD blue (I_+) and red (I_-) detuned from the cavity, as a function of the bath temperature T . For all the simulations, the absolute value of QD-cavity detuning is kept at 10κ .

by the National Science Foundation and Army Research Office. A.M. was supported by the Stanford Graduate Fellowship (Texas Instruments fellowship).

I. SUPPLEMENTARY MATERIALS

A. Derivation of Decay Terms

We use the level diagram as shown in Fig. 1 a to model the effect of phonons explicitly. The Hamiltonian of the system is given by

$$H = H_0 + H_I \quad (12)$$

where,

$$H_0 = \omega_1|1\rangle\langle 1| + \omega_2|2\rangle\langle 2| + \omega_3|3\rangle\langle 3| + \omega a^\dagger a + \sum_j \nu_j b_j^\dagger b_j \quad (13)$$

and

$$H_I = g_v(a|3\rangle\langle 1| + a^\dagger|1\rangle\langle 3|) + \sum_j g_{23}^j(b_j^\dagger|3\rangle\langle 2| + b_j|2\rangle\langle 3|) \quad (14)$$

where, $|i\rangle\langle i|$ is the population operator for i^{th} level; a is the annihilation operator for the cavity mode; b_j is the annihilation operator for a phonon in the j^{th} mode. ω_i , ω and ν_j are the frequencies of the i^{th} energy level, cavity resonance and a phonon in the j^{th} mode. g_v signifies the interaction strength between the cavity and the virtual

transition and g_{23}^j is the interaction strength between the QD exciton and an j^{th} mode phonon. We note that this interaction Hamiltonian is valid only for the level structure as in Fig. 1 a, where the cavity is at lower energy than the QD. For the situation in Fig. 1 b (where the cavity is of higher energy compared to the QD), the interaction Hamiltonian H_I is given by

$$H_I = g_v(a|3\rangle\langle 1| + a^\dagger|1\rangle\langle 3|) + \sum_j g_{23}^j(b_j|3\rangle\langle 2| + b_j^\dagger|2\rangle\langle 3|) \quad (15)$$

In the following derivation, we will use the situation shown in Fig. 1 a.

If we define the QD resonance frequency as ω_a , then $\omega_a = \omega_2 - \omega_1$; and the cavity frequency is given by $\omega_c = \omega_3 - \omega_1$. Then the QD-cavity detuning is given by $\Delta = \omega_2 - \omega_3$. Defining $\sigma_{ij} = |i\rangle\langle j|$, we can write

$$\begin{aligned} \dot{\sigma}_{13} &= -i[\sigma_{13}, H_0 + H_I] \\ &= -i\omega_c\sigma_{13} - ig_v a(\sigma_{11} - \sigma_{33}) - i \sum_j g_{23}^j b_j^\dagger \sigma_{12} \end{aligned}$$

Similarly,

$$\begin{aligned} \dot{\sigma}_{23} &= -i[\sigma_{23}, H_0 + H_I] \\ &= i\Delta\sigma_{23} - ig_v a\sigma_{21} - i \sum_j g_{23}^j b_j^\dagger (\sigma_{22} - \sigma_{33}) \end{aligned}$$

Separating the slow and the fast components of the operators, we can write

$$\sigma_{13} = \tilde{\sigma}_{13} e^{-i\omega_c t} \quad (16)$$

$$\sigma_{23} = \tilde{\sigma}_{23} e^{-i\omega_j t} \quad (17)$$

$$\sigma_{12} = \tilde{\sigma}_{12} e^{-i(\omega_c - \omega_j)t} \quad (18)$$

$$a = \tilde{a} e^{-i\omega_c t} \quad (19)$$

$$b_j^\dagger = \tilde{b}_j^\dagger e^{-i\omega_j t} \quad (20)$$

Hence the equations governing the dynamics of the system can be written as

$$\dot{\tilde{\sigma}}_{13} = -ig_v \tilde{a}(\tilde{\sigma}_{11} - \tilde{\sigma}_{33}) - i \sum_j g_{23}^j \tilde{b}_j^\dagger \tilde{\sigma}_{12} \quad (21)$$

and

$$\dot{\tilde{\sigma}}_{23} = i(\Delta - \omega_j)\tilde{\sigma}_{23} - ig_v \tilde{a}\tilde{\sigma}_{21} - i \sum_j g_{23}^j \tilde{b}_j^\dagger (\tilde{\sigma}_{22} - \tilde{\sigma}_{33}) \quad (22)$$

As level 3 is a virtual level, it is never populated. Hence by adiabatic elimination, using $\dot{\tilde{\sigma}}_{13} = \dot{\tilde{\sigma}}_{23} = 0$, we obtain

$$\tilde{\sigma}_{23} = \frac{g_v \tilde{a} \tilde{\sigma}_{21} + \sum_j g_{23}^j \tilde{b}_j^\dagger (\tilde{\sigma}_{22} - \tilde{\sigma}_{33})}{\Delta - \omega_j} \quad (23)$$

and

$$\tilde{\sigma}_{12} = \frac{-g_v \tilde{a} (\tilde{\sigma}_{11} - \tilde{\sigma}_{33})}{\sum_j g_{23}^j \tilde{b}_j^\dagger} \quad (24)$$

Using these values, we can find the interaction Hamiltonian. The first term $g_v(a\sigma_{31} + a^\dagger\sigma_{13})$ denotes the coherent dynamics. The second term, which signifies the effect of phonons, can be written as (using the Eqns. 23 and 24)

$$H_{ph} = \sum_j g_{23}^j (b_j^\dagger \sigma_{32} + b_j \sigma_{23}) \quad (25)$$

$$= \sum_j g_{23}^j (\tilde{b}_j^\dagger \tilde{\sigma}_{32} + \tilde{b}_j \tilde{\sigma}_{23}) \quad (26)$$

$$= \sum_j \frac{g_{23}^j g_v}{\Delta - \omega_j} (\tilde{b}_j^\dagger \tilde{a}^\dagger \tilde{\sigma}_{12} + \tilde{b}_j \tilde{a} \tilde{\sigma}_{21}) \quad (27)$$

$$+ \sum_j \frac{(g_{23}^j)^2}{\Delta - \omega_j} (\tilde{\sigma}_{22} - \tilde{\sigma}_{33}) (\tilde{b}_j^\dagger \tilde{b}_j^\dagger + \tilde{b}_j \tilde{b}_j) \quad (28)$$

The second term involves two-phonon processes which are less likely. If we neglect them, we can model the effect of phonons as follows:

$$H_{ph} = \sum_j \frac{g_{23}^j g_v}{\Delta - \omega_j} (\tilde{b}_j^\dagger \tilde{a}^\dagger \tilde{\sigma}_{12} + \tilde{b}_j \tilde{a} \tilde{\sigma}_{21}) \quad (29)$$

We can write this Hamiltonian as

$$H_{ph} = (\tilde{a}^\dagger \tilde{\sigma}_{12} \tilde{\Gamma}^\dagger + \tilde{a} \tilde{\sigma}_{21} \tilde{\Gamma}) \quad (30)$$

where, the operator $\tilde{\Gamma}$ can be written as

$$\tilde{\Gamma} = \sum_j \frac{g_{23}^j g_v}{\Delta - \omega_j} \tilde{b}_j \quad (31)$$

and

$$\Gamma = \sum_j \frac{g_{23}^j g_v}{\Delta - \omega_j} b_j e^{-i\omega_j t} \quad (32)$$

To obtain the familiar Lindblad term, we take the partial trace of the correlation between the reservoir operators over the reservoir variables. The correlation is given by

$$\langle \Gamma^\dagger(t') \Gamma(t) \rangle_R = \sum_j \left| \frac{g_{23}^j g_v}{\Delta - \omega_j} \right|^2 e^{-i\omega_j(t-t')} \langle b_j^\dagger b_j \rangle_R \quad (33)$$

As the operators b_j are bosonic and the system is in thermal equilibrium with a bath at temperature T , using the relation

$$\langle b_j^\dagger b_j \rangle_R = \bar{n}(\omega_j, T) = \frac{1}{e^{\frac{\hbar\omega_j}{k_B T}} - 1} \quad (34)$$

we find

$$\langle \Gamma^\dagger(t') \Gamma(t) \rangle_R = \sum_j \left| \frac{g_{23}^j g_v}{\Delta - \omega_j} \right|^2 e^{-i\omega_j(t-t')} \bar{n}(\omega_j, T) \quad (35)$$

and

$$\langle \Gamma(t') \Gamma^\dagger(t) \rangle_R = \sum_j \left| \frac{g_{23}^j g_v}{\Delta - \omega_j} \right|^2 e^{-i\omega_j(t-t')} (\bar{n}(\omega_j, T) + 1) \quad (36)$$

From the correlation, we find that the phonons with frequency Δ (corresponding to the difference between levels $|2\rangle$ and $|3\rangle$, i.e., QD-cavity mode detuning), have the maximum contribution in the interaction Hamiltonian. In the Born-Markov approximation, we can model the electron-phonon interaction (for Fig. 1 a) as an incoherent decay process by adding two extra terms to the Master equation: $2\gamma_r \bar{n} \mathcal{L}(\sigma^\dagger a)$ and $2\gamma_r (\bar{n} + 1) \mathcal{L}(\sigma a^\dagger)$, γ_r being the effective decay rate of the excited QD state and is given by

$$\gamma_r = \frac{1}{2} \sum_j \left| \frac{g_{23}^j g_v}{\Delta - \omega_j} \right|^2 \quad (37)$$

For the situation shown in Fig. 1 b, the decay terms are given by $2\gamma_r \bar{n} \mathcal{L}(\sigma a^\dagger)$ and $2\gamma_r (\bar{n} + 1) \mathcal{L}(\sigma^\dagger a)$. We note that the different rates in both cases are due to an inherent asymmetry between the absorption and emission rates of the phonons.

B. Derivation of the Mean Field Equations

To find the mean field equations for an operator A from the Master equation, we used the following relation:

$$\frac{d\langle A \rangle}{dt} = \frac{d}{dt} \text{Tr}[A\rho] = \text{Tr} \left[A \frac{d\rho}{dt} \right] \quad (38)$$

For the cavity enhanced phonon process, the mean field equations for a non-zero \bar{n} is given by (when the QD is blue detuned from the cavity)

$$\frac{d\langle \sigma \rangle}{dt} = -\gamma \langle \sigma \rangle - \gamma_r (1 + \langle a^\dagger a \rangle) \langle \sigma \rangle \quad (39)$$

$$\gamma_r \bar{n} (1 + 2\langle a^\dagger a \rangle) \langle \sigma \rangle \quad (40)$$

$$\frac{d\langle \sigma_z \rangle}{dt} = -2\gamma (1 + \langle \sigma_z \rangle) \quad (41)$$

$$-2\gamma_r (1 + \bar{n}) (1 + \langle a^\dagger a \rangle) (1 + \langle \sigma_z \rangle) \quad (42)$$

When the QD is red detuned from the cavity, the mean field equations are:

$$\frac{d\langle \sigma \rangle}{dt} = -\gamma \langle \sigma \rangle - \gamma_r \langle a^\dagger a \rangle \langle \sigma \rangle \quad (43)$$

$$\gamma_r \bar{n} (1 + 2\langle a^\dagger a \rangle) \langle \sigma \rangle \quad (44)$$

$$\frac{d\langle \sigma_z \rangle}{dt} = -2\gamma (1 + \langle \sigma_z \rangle) \quad (45)$$

$$-2\gamma_r \bar{n} (1 + \langle a^\dagger a \rangle) (1 + \langle \sigma_z \rangle) \quad (46)$$

We note that while deriving these mean-field equations, we assume that the cavity and QD operators are uncorrelated and write

$$\langle a^\dagger a \sigma \rangle = \langle a^\dagger a \rangle \langle \sigma \rangle \quad (47)$$

Under weak driving, the approximation holds very well. However, in full quantum optical simulations, we do not

make any assumptions.

-
- [1] K. Hennessy, A. Badolato, M. Winger, D. Gerace, M. Atature, S. Gulde, S. Falt, E. L. Hu, and A. Imamoglu, *Nature* **445**, 896 (2007).
 - [2] D. Press, S. Götzinger, S. Reitzenstein, C. Hofmann, A. Löffler, M. Kamp, A. Forchel, and Y. Yamamoto, *Phys. Rev. Lett.* **98**, 117402 (pages 4) (2007), URL <http://link.aps.org/abstract/PRL/v98/e117402>.
 - [3] M. Kaniber, A. Laucht, A. Neumann, J. M. Villas-Boas, M. Bichler, M.-C. Amann, and J. J. Finley, *Physical Review B (Condensed Matter and Materials Physics)* **77**, 161303 (pages 4) (2008), URL <http://link.aps.org/abstract/PRB/v77/e161303>.
 - [4] D. Englund, A. Majumdar, A. Faraon, M. Toishi, N. Stoltz, P. Petroff, and J. Vučković, *Phys. Rev. Lett.* **104**, 073904 (2010).
 - [5] S. Ates, S. M. Ulrich, A. Ulhaq, S. Reitzenstein, A. Löffler, S. Höfling, A. Forchel, and P. Michler, *Nature Photonics* **3**, 724 (2009).
 - [6] A. Auffeves, J.-M. Gerard, and J.-P. Poizat, *Phys. Rev. A* **79**, 053838 (pages 5) (2009), URL <http://link.aps.org/abstract/PRA/v79/e053838>.
 - [7] Y. Ota, S. Iwamoto, N. Kumagai, and Y. Arakawa, arXiv:0908.0788v1 [cond-mat.mes-hall] (2009).
 - [8] U. Hohenester, *Phys. Rev. B* **81**, 155303 (2010).
 - [9] M. Winger, T. Volz, G. Tarel, S. Portolan, A. Badolato, K. J. Hennessy, E. L. Hu, A. Beveratos, J. Finley, V. Savona, et al., *Phys. Rev. Lett.* **103**, 207403 (pages 4) (2009), URL <http://link.aps.org/abstract/PRL/v103/e207403>.
 - [10] N. Chauvin, C. Zinoni, M. Francardi, A. Gerardino, L. Balet, B. Alloing, L. H. Li, and A. Fiore, *Physical Review B (Condensed Matter and Materials Physics)* **80**, 241306 (pages 4) (2009), URL <http://link.aps.org/abstract/PRB/v80/e241306>.
 - [11] A. Majumdar, A. Faraon, E. D. Kim, D. Englund, H. Kim, P. Petroff, and J. Vučković, *Phys. Rev. B* **82**, 045306 (2010).
 - [12] A. Ulhaq, S. Ates, S. Weiler, S. M. Ulrich, S. Reitzenstein, A. Löffler, S. Höfling, L. Worschech, A. Forchel, and P. Michler, *Phys. Rev. B* **82**, 045307 (2010).
 - [13] E. D. Kim, A. Majumdar, H. Kim, P. Petroff, and J. Vuckovic, *Applied Physics Letters* **97**, 053111 (pages 3) (2010), URL <http://link.aip.org/link/?APL/97/053111/1>.
 - [14] F. P. Laussy, E. del Valle, and C. Tejedor, *Phys. Rev. B* **79**, 235325 (2009).
 - [15] G. Gangopadhyay, S. Basu, and D. S. Ray, *Phys. Rev. A* **47**, 1314 (1993).
 - [16] C. W. Gardiner and P. Zoller, *Quantum Noise* (Springer-Verlag, 2005).
 - [17] S. M. Tan, *Journal of Optics B: Quantum and Semiclassical Optics* **1**, 424 (1999), URL <http://stacks.iop.org/1464-4266/1/i=4/a=312>.
 - [18] M. O. Scully and M. S. Zubairy, *Quantum Optics* (Cambridge University Press, 2005).
 - [19] H. Kamada and T. Kutsuwa, *Phys. Rev. B* **78**, 155324 (2008).